J Therm Anal Calorim (2016) 125:397–405
DOI 10.1007/s10973-016-5339-4

A comparative study on thermal behavior of solid-state light trivalent lanthanide isonicotinates in dynamic dry air and nitrogen atmospheres

W. D. G. Nunes[1] · J. A. Teixeira[1] · A. L. C. S. do Nascimento[1] · F. J. Caires[2] · E. Y. Ionashiro[3] · M. Ionashiro[1]

Received: 23 October 2015 / Accepted: 3 February 2016 / Published online: 24 February 2016

Abstract Characterization, thermal stability, and thermal decomposition of light trivalent lanthanide isonicotinates $Ln(L)_3{\cdot}2H_2O$ (Ln = La to Gd, except Pm; L = isonicotinate) were investigated employing simultaneous thermogravimetry and differential scanning calorimetry (TG–DSC), DSC, infrared spectroscopy (FTIR), evolved gas analysis by TG–DSC coupled to FTIR, elemental analysis, and complexometry. The dehydration of these compounds occurs in a single step, and the thermal decomposition of the anhydrous compounds occurs in one or two (air) and two or three steps (N_2). The final residues of thermal decomposition were CeO_2, Pr_6O_{11}, and Ln_2O_3 (Ln = La, Nd to Gd) in air atmosphere, while in N_2 atmosphere the mass loss is still being observed up to 1000 °C. The results also provided information concerning the gaseous products evolved during the thermal decomposition in dynamic dry air and nitrogen atmospheres.

Keywords Lanthanide isonicotinates · Thermal behavior · Evolved gas analysis

Introduction

The interest in the coordination compounds of lanthanide metals comes from its interesting luminescent, magnetic and electronic properties. The coordination number of lanthanide ions allows designing a variety metal–ligand structures in order to achieve desired properties, based on the known chemistry of these metals. Depending on the ligand, as well as the synthetic route employed, these compounds can manifest different properties, e.g., enhanced luminescence, due to the so-called antenna effect; high porosity, due to the cross-linked three-dimensional arrangement of metal–ligand structure, which leads to interesting catalytic and adsorption properties [1].

Isonicotinic acid (4-pyridinecarboxylic acid), a nicotinic acid isomer, is a compound that contains a six-membered ring with five carbon atoms and one nitrogen (pyridine), which replaces one carbon–hydrogen unit in the benzene ring, and a carboxylic group in the position 4. Its main use is as antituberculosis drug, especially the isoniazid (isonicotinic acid hydrazide), the most effective [2]. In addition, isonicotinic acid and its derivatives are used in the production of pharmaceuticals and agrochemicals. An interesting property of isonicotinic acid is its ability to form three-dimensional polymeric structures with transition metal ions and lanthanides, binding by the nitrogen atom from the pyridine ring, and by the carboxylic group oxygens [3–5]. Some isonicotinic coordination compounds obtained by different synthetic routes and with different structures are well known [6–11]. Some of them presents biological properties, as in preventing intravenous thrombosis [neodymium(III) and samarium(III) isonicotinate]. The terbium(III) compound presents a high luminescence intensity and is a promising compound to create luminescent materials [12].

Electronic supplementary material The online version of this article (doi:10.1007/s10973-016-5339-4) contains supplementary material, which is available to authorized users.

✉ M. Ionashiro
massaoi@yahoo.com.br

[1] Instituto de Química, Universidade Estadual Paulista, CP 355, Araraquara, SP 14801-970, Brazil

[2] Faculdade de Ciências, Universidade Estadual Paulista, Bauru, SP 17033-260, Brazil

[3] Instituto de Química, Universidade Federal de Goiás, Campus Samambaia, Goiânia, GO 74690-900, Brazil

A literature survey reveals some studies of lanthanide isonicotinates, concerning essentially its crystalline structure and luminescence properties. In this way, the synthesis and thermal characterization of lanthanides coordination compounds with isonicotinic acid aim to contribute to this area, providing information of its thermal behavior, crystalline transitions and thermal stability (TG–DSC and DSC); gaseous decomposition products (TG–FTIR), in air and nitrogen atmosphere, until now are unreported on the literature.

Experimental

Materials

The isonicotinic acid with 99 % purity was obtained from Aldrich and used as received. Lanthanide oxides (Ln_2O_3 Ln = La, Nd, Sm, Eu, Gd and Pr_6O_{11}) all from Aldrich with 99.9 % purity were used as lanthanide(III) ions precursors, except for cerium which was used as its nitrate salt [$Ce(NO_3)_3{\cdot}6H_2O$].

Synthesis

Aqueous solution of sodium isonicotinate 0.1 mol L^{-1} was prepared by neutralization of aqueous solution of isonicotinic acid with sodium hydroxide solution 0.1 mol L^{-1} until pH 6.5.

Lanthanide chlorides were prepared from the corresponding metal oxide (except for cerium) by treatment with concentrated hydrochloric acid, following the procedure described in [13]. Cerium(III) was used as its nitrate, and c.a. 0.1 mol L^{-1} aqueous solution of this ion was prepared by direct weighing of the salt.

Solid-state compounds were obtained by adding with stirring 155.0 mL of sodium isonicotinate solution 0.1 mol L^{-1} heated up to near ebullition to 50.0 mL of the respective metal ions solutions 0.1 mol L^{-1}. For all the compounds, the beginning of precipitation was observed after total addition of the ligand solution. Thus, the suspensions of the respective metal isonicotinates were evaporated up to near dryness in a water bath, washed with ethanol/water (2:3) mixture until the elimination of chloride ions (qualitative test with $AgNO_3/HNO_3$ solution), dried at 80 °C in a forced air circulation oven during 12 h, and kept in a desiccator over anhydrous calcium chloride.

Experimental equipment and conditions

In the solid-state, metal ions, hydration water, and isonicotinate contents were determined from TG curves. The metal ions were also determined by complexometry with standard EDTA solution after igniting the compounds to the respective oxides and their dissolution in hydrochloric acid solution [14, 15].

Carbon, nitrogen, and hydrogen contents were determined by microanalytical procedures with a CHN elemental analyzer from PerkinElmer, model 2400, and from TG curves.

X-ray powder patterns were obtained by using a Siemens D-5000 X-ray diffractometer employing CuKα radiation ($\lambda = 1.541$ Å) and setting of 40 kV and 20 mA.

The attenuated total reflectance infrared spectra for sodium isonicotinate and for its metal ion compound were run on a Nicolet iS 10 FTIR spectrophotometer, using ATR accessory with Ge window and DTGS detector. The FTIR spectra were recorded with 32 scans per spectrum at resolution of 4 cm^{-1}.

Simultaneous TG–DSC curves were obtained in a TG–DSC1 Mettler Toledo thermal analysis system. The purge gases were dry air and nitrogen with flow of 50 mL min^{-1}. Heating rate of 10 °C min^{-1} was adopted, with samples weighing about 10.0 mg. Alumina crucibles were used for recording the TG–DSC curves.

The evolved gas analysis (EGA/TG–FTIR) experiments were performed coupling the thermogravimetric analyzer to the FTIR spectrometer Nicolet with a gas cell and DTGS KBr detector. The furnace and the heated gas cell (250 °C) were coupled through a heated (225 °C) 120-cm stainless steel transfer line with internal diameter of 3 mm, both purged with dry air and nitrogen (50 mL min^{-1}). The FTIR spectra were recorded with 16 scans per spectrum at a resolution of 4 cm^{-1}.

The DSC curves were obtained using differential scanning calorimeter, model Q10 form TA Instruments. The purge gases were dry air and nitrogen, with flow rate of 50 mL min^{-1}. A heating rate of 10 °C min^{-1} was adopted with samples weighing about 2 mg. Aluminum crucibles with perforated covers was used for recording the DSC curves.

The DSC–photovisual images were obtained on equipment Mettler Toledo DSC-1 stare system coupled to Olympus digital camera, model SC 30. This camera incorporates a 3.3-megapixel CMOS sensor, optical subassembly mechanic Navitar 1-6232D with 6.5× zoom. The experimental conditions were the same used to obtain the DSC curves.

Results and discussion

The analytical and thermoanalytical (TG) data are shown in Table 1. These results permitted to establish the stoichiometry of these compounds, which are in agreement with the general formula $LnL_3{\cdot}2H_2O$, where Ln represents

Table 1 Analytical and thermoanalytical (TG*) data for $Ln(L)_3{\cdot}2H_2O$ compounds

Compounds	Ln (oxide)/%			L (lost)/%		Water/%		C/%			N/%			H/%			Final Residue
	Calcd.	EDTA	TG	Calcd.	TG	Calcd.	TG	Calcd.	EA	TG	Calcd.	EA	TG	Calcd.	EA	TG	
$La(L)_3{\cdot}2H_2O$	30.10	29.90	30.22	63.24	63.08	6.66	6.70	39.94	40.16	39.87	7.76	7.91	7.77	2.99	2.80	2.98	La_2O_3
$Ce(L)_3{\cdot}2H_2O$	31.73	31.50	31.59	61.63	61.64	6.64	6.77	39.85	39.68	39.93	7.75	7.60	7.77	2.98	3.01	2.99	CeO_2
$Pr(L)_3{\cdot}2H_2O$	31.34	31.25	31.11	62.03	62.20	6.63	6.69	39.79	39.95	39.92	7.74	7.66	7.71	2.97	3.00	2.98	Pr_6O_{11}
$Nd(L)_3{\cdot}2H_2O$	30.78	30.60	30.97	62.63	62.32	6.59	6.71	39.55	39.41	39.66	7.69	7.55	7.71	2.96	2.75	2.95	Nd_2O_3
$Sm(L)_3{\cdot}2H_2O$	31.54	31.66	31.55	61.94	61.72	6.52	6.73	39.11	39.40	39.12	7.60	7.51	7.60	2.92	2.70	2.92	Sm_2O_3
$Eu(L)_3{\cdot}2H_2O$	31.75	31.80	31.42	61.75	61.93	6.50	6.65	39.00	38.75	38.81	7.58	7.67	7.54	2.92	3.00	2.91	Eu_2O_3
$Gd(L)_3{\cdot}2H_2O$	32.39	32.20	32.26	61.17	61.20	6.44	6.54	38.63	38.76	38.70	7.51	7.68	7.50	2.89	2.70	2.90	Gd_2O_3

Ln = light lanthanides; * TG in air atmosphere, L = isonicotinate

light trivalent lanthanides (except promethium) and L is isonicotinate.

XRD

The X-ray diffraction powder patterns (Fig. 1) shows that all the compounds have a crystalline structure, without evidence for formation of isomorphous compounds and the crystallinity of these compounds follows the order Nd > Pr > La ~ Ce > Sm ~ Eu > Gd. The difference in the crystallinity of the compounds must be due to precipitation conditions, which were not controlled.

Infrared spectroscopy

The attenuated total reflectance infrared spectroscopic data on isonicotinate (sodium salt) and its compounds with the metal ions considered in this work are shown in Fig. 2. The investigation was focused mainly in the 1700–1400 cm^{-1} range, because this region is potentially most informative in attempting to assign coordination sites, and the frequencies of interest are shown in Table 2.

In isonicotinate (sodium salt), medium-intensity band at 1542 cm^{-1} and a strong band at 1410 cm^{-1} are attributed to the antisymmetric ($\nu_{as}CO_2^-$) and symmetric ($\nu_{sym}CO_2^-$) stretching frequencies of carboxylate groups, respectively [16, 17]. For the synthesized compounds, these frequencies are located between 1547–1539 and 1414–1404 cm^{-1}, respectively. Analysis of the frequencies of the $\nu_{as}CO_2^-$ and $\nu_{sym}CO_2^-$ indicates that the coordination is carried out through the carboxylate [16] and the infrared spectra data suggest that the bonding of the carboxylate group to metal is bridging bidentate [18].

Thermal analysis

TG–DSC in dry air atmosphere

The simultaneous TG–DSC curves of the compounds in dry air atmosphere are shown in Fig. 3. These curves show mass losses in two or three steps and endothermic peaks attributed to dehydration, thermal decomposition, or physical phenomenon and exothermic peaks attributed to oxidation of the organic matter and/or of the gaseous products evolved during the thermal decomposition.

The thermal stability of the hydrated compounds (I) or anhydrous ones (II) and the final temperature of thermal decomposition (III), as well as the dehydration temperature range (IV) as shown by the TG–DSC curves, depend on the nature of the metal ion, and they follow the order:

(I) Sm > La = Ce = Pr = Nd = Eu > Gd

(II) La > Pr > Eu > Nd > Sm > Gd > Ce

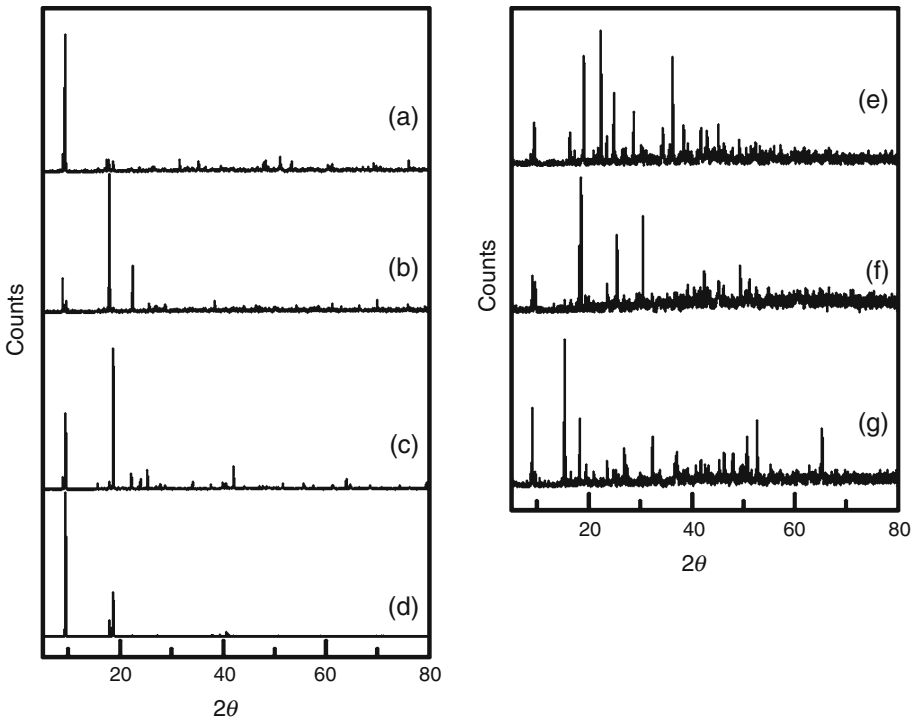

Fig. 1 X-ray powder diffractograms: (*a*) $LaL_3{\cdot}2H_2O$; (*b*) $CeL_3{\cdot}2H_2$; (*c*) $PrL_3{\cdot}2H_2O$; (*d*) $NdL_3{\cdot}2H_2O$; (*e*) $SmL_3{\cdot}2H_2O$; (*f*) $EuL_3{\cdot}2H_2O$; (*g*) $GdL_3{\cdot}2H_2O$

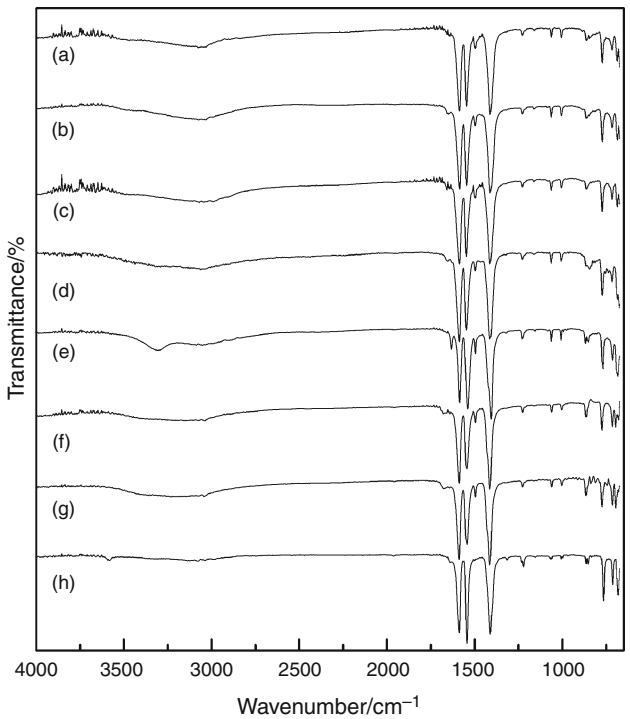

Fig. 2 FTIR spectra of: (*a*) $LaL_3{\cdot}2H_2O$; (*b*) $CeL_3{\cdot}2H_2$; (*c*) $PrL_3{\cdot}2H_2O$; (*d*) $NdL_3{\cdot}2H_2O$; (*e*) $SmL_3{\cdot}2H_2O$; (*f*) $EuL_3{\cdot}2H_2O$; (*g*) $GdL_3{\cdot}2H_2O$; (*h*) NaL

(III) Pr > Sm > La > Nd = Eu = Gd > Ce

(IV) Sm > Nd > Pr > Ce > La > Eu = Gd

Table 2 Experimental spectroscopic data for sodium isonicotinate and its compounds with light trivalent lanthanides ions, except promethium

Compounds	FTIR		
	$\nu_{as}^{(CO_2^-)}/cm^{-1}$	$\nu_{sym}^{(CO_2^-)}/cm^{-1}$	$\Delta\nu/cm^{-1}$
NaL	1542	1410	132
$LaL_3{\cdot}2H_2O$	1547	1412	135
$CeL_3{\cdot}2H_2O$	1545	1411	134
$PrL_3{\cdot}2H_2O$	1546	1413	133
$NdL_3{\cdot}2H_2O$	1547	1414	133
$SmL_3{\cdot}2H_2O$	1539	1404	135
$EuL_3{\cdot}2H_2O$	1543	1414	129
$GdL_3{\cdot}2H_2O$	1543	1414	129

L isonicotinate, $\nu_{as}^{(COO^-)}$ carboxylate asymmetric stretching frequency, $\nu_{sym}^{(COO^-)}$ carboxylate symmetric stretching frequency, $\Delta\nu$ difference between $\nu_{as}^{(COO^-)}$ and $\nu_{sym}^{(COO^-)}$ frequencies

These curves also show that all the compounds were obtained as dihydrated and the dehydration occurs in a single step. Three patterns of thermal behavior are observed for the compounds. Firstly, a close similarity is noted concerning the TG–DSC profiles of lanthanum and neodymium to gadolinium Fig. 3a, d–g. On the other hand, cerium and praseodymium, Fig. 3b, c, display a TG–DSC profile characteristic for each compound. Thus, the features of each compound are discussed based on their similar thermal profiles.

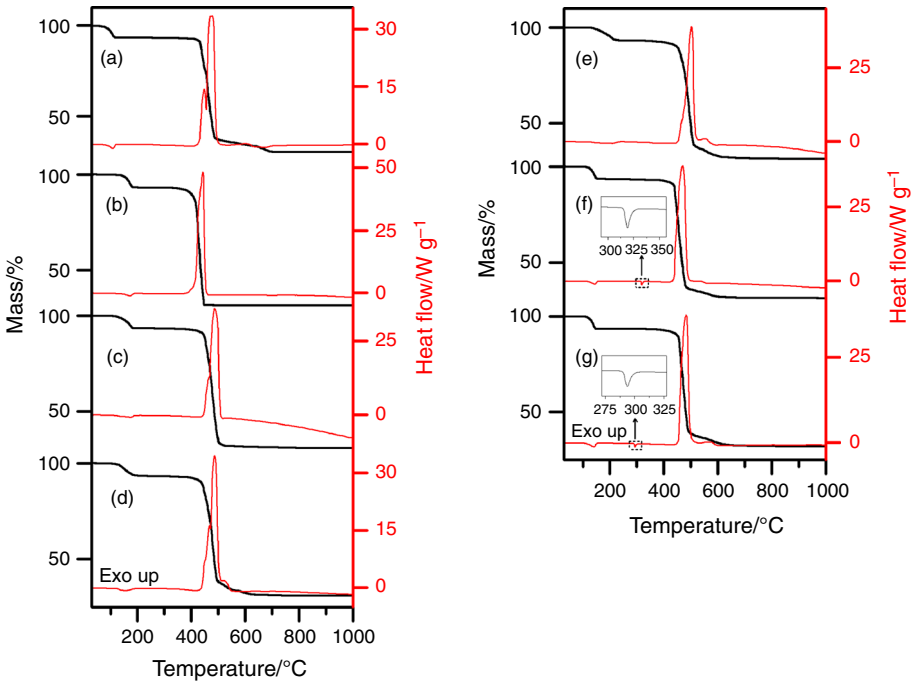

Fig. 3 TG–DSC curves in dynamic dry air atmosphere. (*a*) $LaL_3{\cdot}2H_2O$ (10.0172 mg); (*b*) $CeL_3{\cdot}2H_2O$ (10.0184 mg); (*c*) $PrL_3{\cdot}2H_2O$ (10.0822 mg); (*d*) $NdL_3{\cdot}2H_2O$ (9.9793 mg); (*e*) $SmL_3{\cdot}2H_2O$ (9.9682 mg); (*f*) $EuL_3{\cdot}2H_2O$ (10.0662 mg); (*g*) $GdL_3{\cdot}2H_2O$ (10.0952 mg)

Cerium compound

The TG–DSC curves are shown in Fig. 3b. The first mass loss between 110 and 180 °C, corresponding to an endothermic peak at 170 °C, is attributed to dehydration, with loss of 2 H_2O molecules (Calcd. = 6.64 %, TG = 6.77 %). The anhydrous compound is stable up to 340 °C, and above this temperature the thermal decomposition occurs in a single step and through a fast process up to 450 °C. The broad and sharp exothermic peak at 440 °C, corresponding to this mass loss is attributed to oxidation reaction of Ce(III) to Ce(IV), together with the oxidation of the organic matter and/or the gaseous products evolved during the thermal decomposition. The smaller thermal stability of the cerium compound undoubtedly is due to oxidation reaction of Ce(III) and had already been observed for other cerium compound [19]. The total mass loss up to 450 °C is in agreement with the formation of cerium(IV) oxide, CeO_2, as final residue (Calcd. = 68.27 %, TG = 68.41 %).

Praseodymium compound

The TG–DSC curves are shown in Fig. 3c. The first mass loss between 110 and 190 °C, corresponding to a small and broad endothermic event (120–190 °C), is attributed to dehydration, with loss of 2 H_2O molecules (Calcd. = 6.63 %, TG = 6.69 %). The anhydrous compound is stable up to 400 °C, and above this temperature the thermal decomposition occurs in two steps between 400–510 and 510–720 °C, with losses of 61.14 and 1.06 %, respectively. The first step that occurs through a fast process, corresponding to a large and sharp exothermic peak at 490 °C with shoulder at 470 °C is attributed to oxidation of organic matter and/or gaseous products evolved during the thermal decomposition together with the oxidative reaction of Pr(III) to Pr_6O_{11}, with formation of small amount of carbonaceous residue.

The last step is attributed to oxidation of carbonaceous residue. No thermal event is observed in this step because the heat involved is not sufficient to produce a thermal event, undoubtedly due to the small amount of residue and the mass loss that occurs slowly. The total mass loss up to 720 °C is in agreement with the formation of praseodymium oxide, Pr_6O_{11}, as final residue (Calcd. = 62.03 %; TG = 62.20 %).

Lanthanum and neodymium to gadolinium compounds

The TG–DSC curves are shown in Fig. 3a, d–g. For all the compounds the first mass loss between 110–175 °C (La), 110–200 °C (Nd), 125–230 °C (Sm), 110–160 °C (Eu), and 105–155 °C (Gd), corresponding to an endothermic peak at 170 °C (La), 145 °C (Eu), 140 °C (Gd), and a small and broad endothermic event around 150 °C (Nd) and 210 °C (Sm) is attributed to dehydration with loss of 2 H_2O (Calcd., TG: La = 6.66 %, 6.70 %; Nd = 6.59 %, 6.71 %; Sm = 6.52 %, 6.73 %; Eu = 6.50 %, 6.65 %; Gd = 6.44 %, 6.54 %).

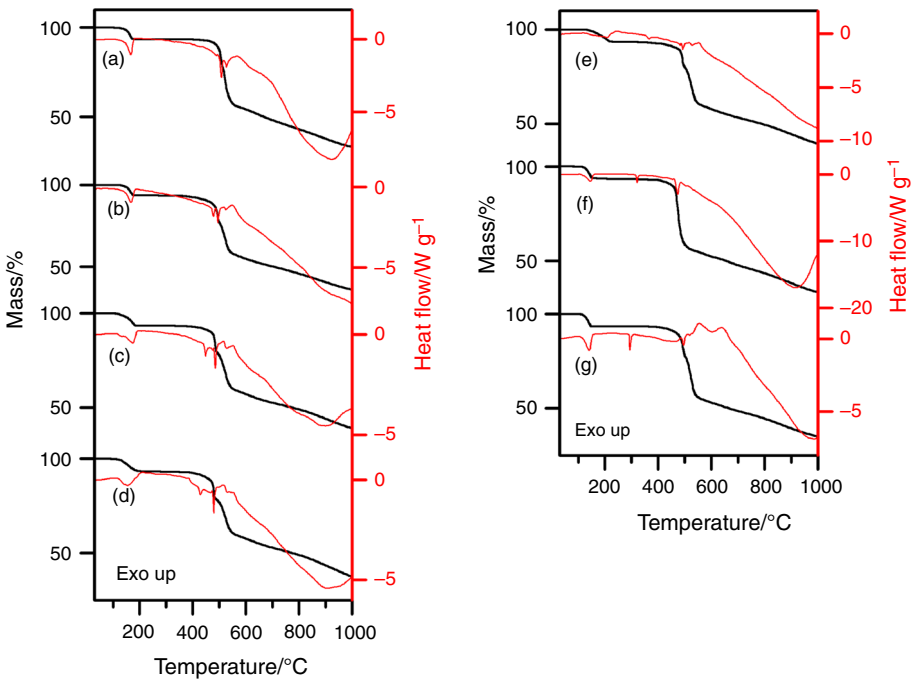

Fig. 4 TG–DSC curves in N_2 atmosphere. (*a*) $LaL_3{\cdot}2H_2O$ (10.0527 mg); (*b*) $CeL_3{\cdot}2H_2O$ (10.0066 mg); (*c*) $PrL_3{\cdot}2H_2O$ (9.9927 mg); (*d*) $NdL_3{\cdot}2H_2O$ (9.9977 mg); (*e*) $SmL_3{\cdot}2H_2O$ (10.0018 mg); (*f*) $EuL_3{\cdot}2H_2O$ (10.0170 mg); (*g*) $GdL_3{\cdot}2H_2O$ (10.0213 mg)

The anhydrous compounds are stable up to 430 °C (La), 370 °C (Nd), 360 °C (Sm), 375 °C (Eu), and 345 °C (Gd), and above these temperatures the thermal decomposition occurs in two consecutive steps. For lanthanum and neodymium compounds, the first step occurs between 430–515 °C (La) and 370–510 °C (Nd) although the DSC curves suggest two overlapping steps, the mass loss occurs through a fast process with loss of 55.63 and 55.45 % respectively. For samarium, europium, and gadolinium compounds the first step between 360–520 °C (Sm), 375–490 °C(Eu), and 345–495 °C (Gd), and the mass loss also occurs through a fast process with loss of 55.18, 56.49, and 54.46 %, respectively.

The exothermic peaks at 470 and 495 °C (La), 470 and 490 °C (Nd), 505 °C (Sm), 470 °C (Eu), and 485 °C (Gd) are attributed to oxidation of the organic matter and/or the gaseous products evolved during the thermal decomposition, with the formation of carbonaceous residue and a derivative of carbonate, which were confirmed by tests with hydrochloric acid solution on sample heated up to the temperature indicated by TG–DSC curves.

The last step that occurs through a slow process, between 510–695 °C (La), 510–690 °C (Nd), 520–715 °C (Sm), 490–690 °C (Eu), and 495–690 °C (Gd) with loss of 7.45, 6.87, 6.54, 5.44, and 6.74 %, corresponding to an exothermic event at 570, 610, 530, 555, 540, and 570 °C, respectively, followed by an endothermic between 630–690 °C (La), 550–610 °C (Nd), 590–620 °C (Sm), 555–590 °C (Eu), and 590–620 °C (Gd) attributed to oxidation of the carbonaceous residue and the thermal decomposition of derivative of carbonate.

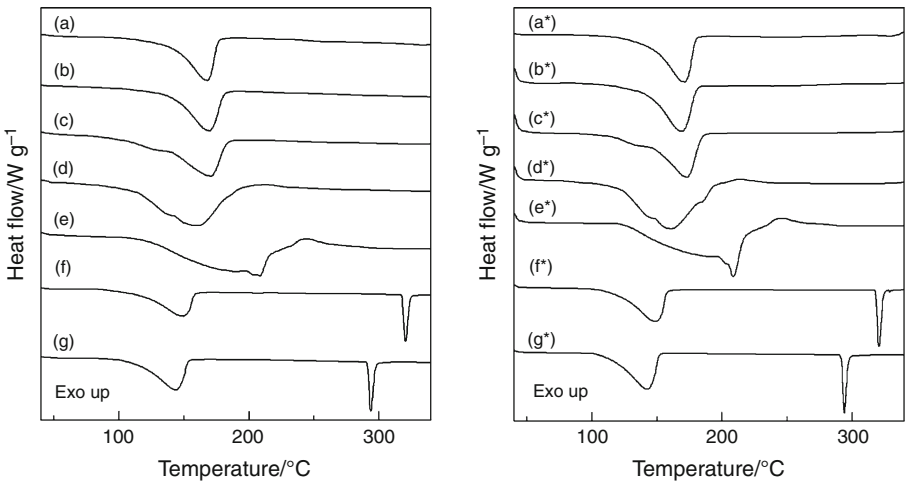

Fig. 5 DSC curves in dry air (*a*–*g*) and N_2 (*a**–*g**) atmospheres. (Sample mass: air/N_2): (*a*) $LaL_3{\cdot}2H_2O$ (2.063/2.054 mg); (*b*) $CeL_3{\cdot}2H_2O$ (2.089/2.048 mg); (*c*) $PrL_3{\cdot}2H_2O$ (2.049/2.050 mg); (*d*) $NdL_3{\cdot}2H_2O$ (2.141/2.155 mg); (*e*) $SmL_3{\cdot}2H_2O$ (2.024/2.041 mg); (*f*) $EuL_3{\cdot}2H_2O$ (2.141/2.180 mg); (*g*) $GdL_3{\cdot}2H_2O$ (2.148/2.175 mg)

The total mass loss of these compounds up to the minimum oxide level temperatures are in agreement with the formation of the respective oxides, Ln_2O_3 (Ln = La, Nd, Sm, Eu and Gd) (Calcd., TG: La = 63,24 %, 63,08 %; Nd = 62.63 %, 62,32 %; Sm = 61.94 %, 61.72 %; Eu = 61.75 %, 61.93 %; Gd = 61.17 %, 61.21 %).

TG–DSC in N_2 atmosphere

The TG–DSC curves in dry nitrogen atmosphere are shown in Fig. 4. These curves show mass losses in three (Eu) or four (La to Sm and Gd) steps and endothermic peaks attributed to dehydration, pyrolysis and physical phenomenon or without thermal event.

The thermal stability of the hydrated compounds (I) or anhydrous ones (II) and the final temperature of thermal decomposition (III) as shown by the TG–DSC curves are not the same from that observed in dry air atmosphere, and they follow the order:

(I) Sm > La > Ce = Eu > Gd > Pr = Nd
(II) La > Pr > Gd > Eu > Nd = Sm > Ce

For all the compounds, these curves also show that the mass loss is still being observed up to 1000 °C, and except for europium, a great similarity is observed concerning the TG–DSC profiles of these compounds, Fig. 4a–e, g. On that account, the features of each compound are also discussed based on these similar profiles.

Europium compound

The TG–DSC curves are shown in Fig. 4f. The first mass loss between 110 and 160 °C, corresponding to an endothermic peak at 145 °C, is attributed to dehydration, with loss of 2 H_2O molecules (Calcd. = 6.50 %, TG = 6.59 %).

The anhydrous compounds are stable up to 380 °C, and above this temperature the thermal decomposition occurs in two consecutive steps between 380–520 and 520–>1000 °C, with losses of 36,91 and >22,76 %, corresponding to endothermic peaks at 475 and 915 °C attributed to thermal decomposition of the compounds and pyrolysis of the carbonaceous residue.

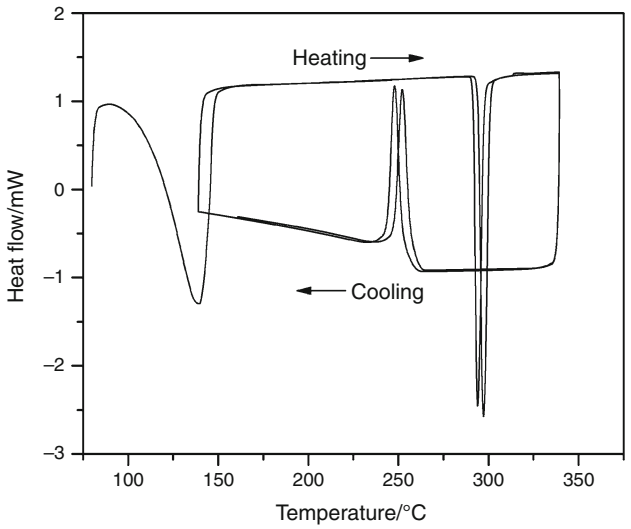

Fig. 6 DSC cycle (heating/cooling/heating/cooling) of gadolinium compound, showing the exothermic peak on cooling attributed to the reversible phase transition

Lanthanum to samarium and gadolinium compounds

The TG–DSC curves are shown in Fig. 4a–e, g. For all the compounds, the first mass loss between 120–180 °C (La), 110–180 °C (Ce), 100–190 °C (Pr), 100–210 °C (Nd), 130–210 °C (Sm), and 105–150 °C (Gd), corresponding to an endothermic peak at 170 °C (La, Ce), 175 °C (Pr), 155 °C (Nd), 140 °C (Gd) and an endotherm between 130–220 °C (Sm), is attributed to dehydration with loss of 2 H_2O molecules (La to Sm, Gd; Calcd. = 6.66, 6.64, 6.63, 6.59, 6.52, 6.44 %; TG = 6.65, 6.61, 6.57, 6.85, 6.66, 6.59, 6.51 %, respectively).

The anhydrous compounds (La to Sm, Gd) are stable up to 420, 315, 400, 370, 370, 390 °C, and above these temperatures the thermal decomposition occurs in three consecutive steps between 420–510, 510–560, and 560–>1000 °C (La); 315–500, 500–550, and 550–>1000 °C (Ce); 400–490, 490–555, and 555–>1000 °C (Pr); 370–485, 485–560, and 560–>1000 °C (Nd); 370–490, 490–550, and 550–>1000 °C (Sm); 390–500, 500–545, and 545–>1000 °C (Gd), respectively. The first two steps that occur through fast processes with losses of 5.54 and 22.71 % (La), 15.81 and 19.44 % (Ce), 13.51 and 20.26 % (Pr), 14.21 and 18.94 % (Nd), 13.03 and 19.67 % (Sm), 15.85 and 21.44 % (Gd) corresponding to endothermic peaks at 490, 510 and 525 °C (La), 480, 495, and 595 °C (Ce), 450, 480, 485, and 530 °C(Pr), 430, 465, 480, and 530 °C (Nd), 480, 495, and 530 °C (Sm), 495 and 520 °C (Gd), attributed to the thermal decomposition and formation of carbonaceous residue.

The last mass loss that occurs slowly and is still being observed up to 1000 °C is attributed to the pyrolysis of the carbonaceous residue.

In both atmospheres (air, N2), the endothermic peak at 370 °C (Sm), 320 °C (Eu), and 275 °C (Gd) without mass loss in TG curve is attributed to irreversible phase transition.

DSC

The DSC curves in nitrogen and air atmospheres, measured up to 350 °C, are shown in Fig. 5a–g and Fig. 5a*–g*, respectively. In both atmospheres (air, N_2) these curves show endothermic peaks at 171 and 168 °C (La), 170 °C (Ce) 173

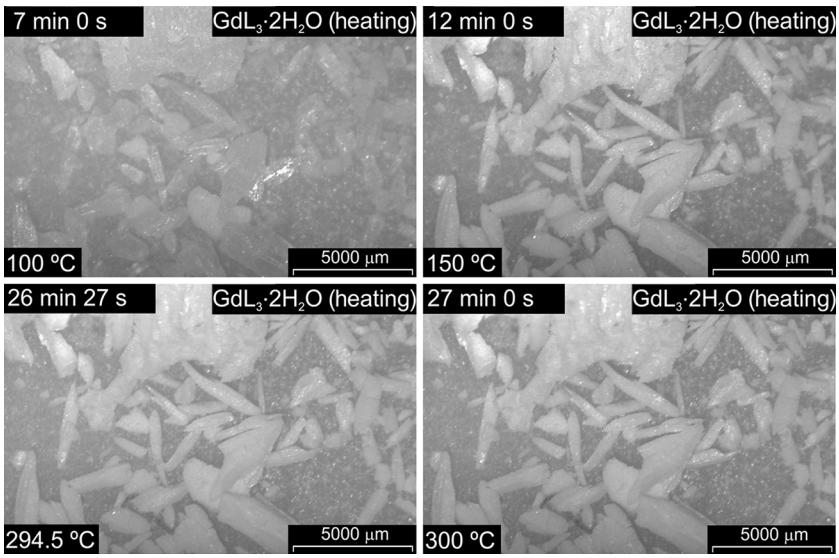

Fig. 7 DSC–photovisual micrographs of $GdL_3{\cdot}2H_2O$ showing the crystal change on dehydration (*upper left/right*) and phase transition (*bottom left/right*)

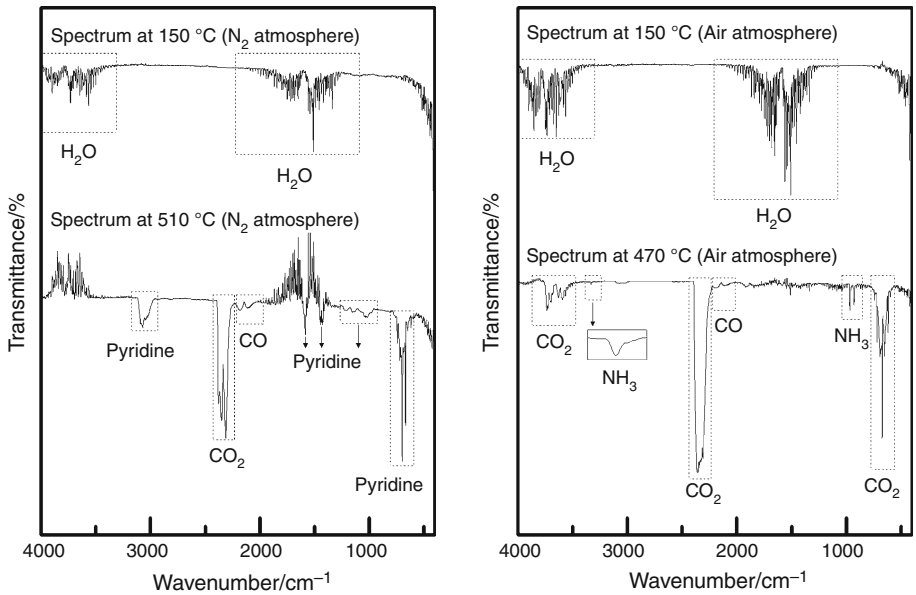

Fig. 8 FTIR spectra of gases evolved during thermal decomposition of Lanthanum compound ($LaL_3{\cdot}2H_2O$), in air and N_2 atmospheres

and 171 °C (Pr), 161 and 160 °C (Nd), 209 °C (Sm), 250 °C (Eu), 143 and 144 °C (Gd) attributed to dehydration, and at 321 (Eu) and 294 °C (Gd) due to reversible phase transition. The dehydration enthalpies calculated for these compounds were 103.6 and 110.6 (La), 110.6 and 106.3 (Ce), 121.0 and 119.3 (Pr), 129.8 and 139.8 (Nd), 161.9 and 177.7 (Sm), 108.9 and 106.1 (Sm), 109.5 and 108.3 (Gd) kJ mol^{-1}, in air and N_2 atmospheres, respectively.

For europium and gadolinium compounds, the reversible phase transition enthalpies were 26.4 and 27.1 (Eu), 26.0 and 26.0 (Gd) kJ mol^{-1}, in air and N_2 atmospheres, respectively. The reversibility of phase transition was confirmed by DSC heating/cooling cycles for the compounds, as indicated by the exothermic peaks observed around 250 °C in Fig. 6. Only the gadolinium compound DSC curves are shown as representative.

The DSC–photovisual micrograph shows visible changes in the crystal aspect, while the gadolinium compound is heated, as illustrated in Fig. 7. The first thermal event attributed to dehydration ($\sim$140 °C) causes a slight change in the crystal opacity, passing from slightly translucent to an opaque white color, Fig. 7 (upper left/right). At about 295 °C, the compound pass through the phase transition and it is possible to observe the contraction of the crystals, possibly due to a rearrangement of the crystal lattice, as illustrated in Fig. 7 (bottom left/right). On cooling it is also

possible to observe the reverse phenomenon at around 250 °C, but this time only a slight change on the position of the crystals is visible. For more details see the video in supplementary material.

Evolved gas analysis

The gaseous products evolved during the thermal decomposition of light trivalent lanthanide isonicotinates in both atmospheres were monitored by FTIR, and in all the compounds were detected ammonia, carbon monoxide and carbon dioxide (air) or pyridine, carbon monoxide and carbon dioxide (N_2). The IR spectra of gaseous products detected during thermal decomposition of Lanthanum compound, as representative of all the synthesized compounds in this work are shown in Fig. 8.

Conclusions

From TG, complexometry, and elemental analysis data, a general formula could be established for the synthesized compounds.

The infrared spectroscopic data suggest that the isonicotinate act as a bridging bidentate ligand toward the light trivalent lanthanides.

The monitoring of evolved gases (EGA) shows that during the thermal decomposition the compounds occurs the release of ammonia, CO and CO_2 (air) and pyridine, CO and CO_2 (N_2).

From DSC and DSC–photovisual analysis, it was possible to measure the enthalpies of dehydration and evaluate the reversibility of the phase transitions for gadolinium and europium compounds.

The TG–DSC and DSC curves also provided previously unreported information about the thermal stability and thermal decomposition in dynamic dry and nitrogen atmospheres.

Acknowledgements The authors thank FAPESP (Proc. 2013/09022-7), CNPq, and CAPES foundations (Brazil) for financial support.

References

1. De Sá GF, Malta OL, de Mello Donegá C, Simas AM, Longo RL, Santa-Cruz PA, et al. Spectroscopic properties and design of highly luminescent lanthanide coordination complexes. Coord Chem Rev. 2000. http://www.sciencedirect.com/science/article/pii/S0010854599000545.
2. Van Loenhout-Rooyackers JH, Veen J. Treatment of pulmonary tuberculosis. Neth J Med. 1998;53:7–14. http://www.sciencedirect.com/science/article/pii/S0300297798000679.
3. Lin CZJ, Chui SSY, Lo SMF, Shek FLY, Wu M, Suwinska K, et al. Physical stability vs. chemical lability in microporous metal coordination polymers: a comparison of [Cu(OH)(INA)]n and [Cu(INA)2]n: INA = 1,4-($NC_5H_4CO_2$). Chem Commun (Camb). 2002;1:1642–3.
4. Duan LM, Lin CK, Wang H, Liu XM, Lin J. Syntheses, structures and luminescence properties of five lanthanide-isonicotinate coordination polymers. Inorg Chim Acta. 2010;363:1507–12. doi:10.1016/j.ica.2010.01.018.
5. Almeida Paz FA, Klinowski J. Hydrothermal synthesis of a novel thermally stable three-dimensional ytterbium-organic framework. Chem Commun. 2003. doi:10.1039/B302140H.
6. Chen W, Fukuzumi S. Ligand-dependent ultrasonic-assistant self-assemblies and photophysical properties of lanthanide nicotinic/isonicotinic complexes. Inorg Chem. 2009;48:3800–7.
7. Jia G, Law GL, Wong KL, Tanner PA, Wong WT. Synthesis, crystal structures, and luminescence of organic-lanthanide complexes with nicotinate and isonicotinate ligands. Inorg Chem. 2008;47:9431–8.
8. Huang L, Han L, Zhu D, Chen L, Xu Y. Hydrothermal synthesis, crystal structure and luminescence of two new 2D coordination polymers [Ln(IN)(CO_3)(H_2O)] (LnLa, Eu) constructed by interesting flat lanthanide carbonate layers. Inorg Chem Commun. 2012;21:80–3. doi:10.1016/j.inoche.2012.04.018.
9. Naumova MI, Manicheva EA, Geraski OA, Fedin VP. Synthesis and crystal structures of new lanthanide isonicotinates: coordination polymers and molecular complexes. Russ Chem Bull. 2009;58:1858–65.
10. Hilder M, Lezhnina M, Junk PC, Kynast UH. Spectroscopic properties of lanthanoid benzene carboxylates in the solid state: Part 3. N-heteroaromatic benzoates and 2-furanates. Polyhedron. 2013;52:804–9. doi:10.1016/j.poly.2012.07.047.
11. Yan B, Zhou B. Photophysical properties of dysprosium complexes with aromatic carboxylic acids by molecular spectroscopy. J Photochem Photobiol A Chem. 2005;171:181–6.
12. Ma L, Evans OR, Foxman BM, Lin W. Luminescent lanthanide coordination polymers. Inorg Chem. 1999;38:5837–40.
13. Colman TAD, Gomes DJC, Caires FJ, Filho OT, da Silva RDC, Ionashiro M. Synthesis, thermal and spectroscopic study of light lanthanide nicotinate, in the solid state. Thermochim Acta. 2014;591:111–8. http://linkinghub.elsevier.com/retrieve/pii/S0040603114002743.
14. Ionashiro M, Graner CAF, Netto JZ. Titulação complexométrica de lantanídeos e ítrio. Eclet Quim. 1983;8:29–32.
15. Flaschka HA. EDTA titrations. Oxford: Pergamon Press; 1964.
16. Nakamoto K. Infrared and Raman Spectra of Inorganic and Coordination Compounds, Part B. 5th ed. New York: Wiley; 1997.
17. Silverstein RM, Webster FX. Spectrometric identification of organic compounds. 6th ed. New York: Wiley; 1998.
18. Deacon GB, Phillips RJ. Relationships between the carbon–oxygen stretching frequencies of carboxylato complexes and the type of carboxylate coordination. Coord Chem Rev. 1980;33:227–50. http://www.sciencedirect.com/science/article/pii/S0010854500804555.
19. Lima LS, Caires FJ, Carvalho CT, Siqueira AB, Ionashiro M. Synthesis, characterization and thermal behaviour of solid-state compounds of light trivalent lanthanide succinates. Thermochim Acta. 2010;501:50–4. doi:10.1016/j.tca.2010.01.001.